analytical chemistry

Letter

pubs.acs.org/ac

Regulation of DNA Self-Assembly and DNA Hybridization by Chiral Molecules with Corresponding Biosensor Applications

Benmei Wei,[†] Nannan Liu,[†] Juntao Zhang,[†,‡] Xiaowen Ou,[†] Ruixue Duan,[†] Zekun Yang,[†] Xiaoding Lou,[†] and Fan Xia*[,†,‡]

[†]Key Laboratory for Large-Format Battery Materials and System, Ministry of Education, School of Chemistry and Chemical Engineering, Huazhong University of Science and Technology, Wuhan, Hubei 430074, P. R. China

[‡]National Engineering Research Center for Nanomedicine, College of Life Science and Technology, Huazhong University of Science and Technology, Wuhan, Hubei 430074, P. R. China

Supporting Information

ABSTRACT: Chirality is one of the fundamental biochemical properties in a living system, and a lot of biological and physiological processes are greatly influenced by the chirality of molecules. Inspired by this phenomenon, we study the covalent assembly of DNA on chiral molecule modified surfaces and further discuss the hybridization of DNA on chiral surfaces with nucleic acids. Take methylene blue (MB) modified DNA as a model molecule, we show that the peak current of the L-NIBC (NIBC, *N*-isobutyryl-L(D)-cysteine) modified gold surface (L-surface) is larger than the D-surface because of a stronger interaction between short-chain DNA and the L-surface; however, the D-surface has a higher hybridization efficiency than the L-surface. Moreover, we apply this result to actual application by choosing an electrochemical DNA (E-DNA) sensor as a potential platform. Furthermore, we further amplify the difference of hybridization efficiency using the supersandwich assay. More importantly, our findings are successfully employed to program the sensitivity and limit of detection.

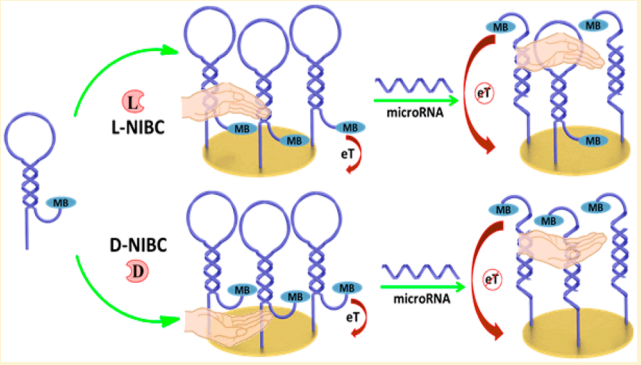

Chirality is one of the fundamental biochemical properties in the living world.[1−3] Most of the biological molecules (proteins, RNA, DNA, etc.) are composed of small chiral biomolecules (e.g., L-amino acids, D-sugars, L-phospholipids, etc.). As a result, a lot of biological and physiological processes are greatly influenced by the chirality of molecules. For example, *R*-thalidomide has a sedative effect, whereas *S*-thalidomide would cause serious side effects on fetal development, which led to more than ten thousand women giving birth to children with deformities after using racemic thalidomide in the last century.[4] Many groups have investigated the interaction between biomolecules and chiral molecules in view of the significance of chirality in the living systems.[5−19] For instance, Sun and co-workers have observed that long-chain single-stranded[10] and double-stranded DNAs[11] (at least 3000 bases) exhibit different interactions with chiral *N*-isobutyryl-L(D)-cysteine (NIBC) modified gold surfaces. They find that DNA molecules have a much stronger interaction with the L-NIBC coated gold surface compared to the corresponding D-NIBC coated gold surface. In addition, they and other groups discovered the different cell behaviors,[12−14] protein adsorption,[15,16] and other biological processes[17−19] on enantiomorphous surfaces. Despite their many positive attributes in the past few years, these studies mainly focus on investigating different adsorption mechanisms on enantiomorphous surfaces. Moreover, the different biomolecular adsorption processes on chiral surfaces is only a starting point, and many intriguing chiral phenomena associated with chiral molecules in the biological world remain poorly understood.

DNA is the master biomolecular of every cell and contains vital information that gets passed on to each successive generation. DNA adsorption is important, but DNA self-assembly is even more important in consideration of the actual application. Self-assembly monolayers or multilayers are crucially important in the development of life science, nanotechnology, and so on.[20−22] In particular, the self-assembly monolayer of DNA has been successfully applied in biosensors,[23−26] molecular machines,[27,28] and complex nanoarchitectures.[29,30] In general, the fabrication of the DNA monolayer is realized through the covalent coupling method, which has the advantage of high mechanical rigidity and chemical stability. Moreover, the covalent assembly of DNA has a great significance on DNA surface array and hybridization. To the best of our knowledge, there is no report on the regulation of DNA assembly by molecular chirality, let alone DNA hybridization. Therefore, study of the covalent immobilization

Received: December 18, 2014
Accepted: February 3, 2015

DOI: 10.1021/ac504797e
Anal. Chem. XXXX, XXX, XXX−XXX

of DNA and further investigation of the DNA hybridization on chiral molecule modified surfaces are of interest since it would enable great development in DNA-based biosensors, nanodevices, and biochips.

Here, we report the regulation of DNA self-assembly and DNA hybridization by molecular chirality. First, we investigate the covalent assembly of DNA on enantioselective gold surfaces. Second, we further discuss the hybridization of DNA on chiral surfaces with nucleic acids. Third, we design a stem-loop structure probe (molecular beacon) for the detection of nucleic acid and investigate the difference of hybridization efficiency on chiral molecular modified electrochemical DNA (E-DNA) sensors.[31−33] Finally, we perform the DNA detection using a one-dimensional structure (supersandwich) and obtain a significant difference on the enantioselective sensors.

Previous studies have proven that long-chain DNA shows different interactions with chiral molecule coated gold surfaces, leading to a fact that long-chain DNA has a larger adsorption quality on the L-NIBC modified gold surface (L-surface) than the D-surface.[10,11] Because all probes and targets of E-DNA sensors are composed of short-chain nucleic acids, we choose a short-chain DNA (23 bases) as a model molecule to investigate DNA adsorption on L/D-surfaces by quartz crystal microbalance (QCM), in which the absorbed mass has a liner relationship with the frequency decrease of the quartz crystal resonator.[34] The result shows that the L-surface exhibits a much large frequency shift than the D-surface (Figure S1c, Supporting Information). We also discuss the DNA adsorption on enantioselective gold surfaces by cyclic voltammetry (CV), which is an effective and sensitive method for investigating the feature of the electrode surface (Figure S1d, Supporting Information). The electrochemical responses of L- and D-surfaces are almost the same after the electrodes are immersed in 1 μM L-NIBC and D-NIBC, respectively, meaning the assembly quality of chiral molecules on gold surfaces is almost identical. Meanwhile, the peak currents are decreased after L- and D-surfaces are treated with DNA, indicating the adsorbed DNA insulated the interfacial electron transfer. However, the decrease of peak current of the L-surface is larger than the D-surface, hinting that the adsorbed DNA molecules on the L-surface is higher. The above results confirm that short-chain DNA has a larger adsorption quality on the L-surface than the D-surface; namely, the L-surface may have a stronger H-bond interaction with short-chain DNA. At the same time, these conclusions are consistent with long-chain DNA observation.

To investigate the influence of surface chirality on the covalent assembly of DNA, we choose a thiolated methlyene blue (MB)-modified stem-loop structure DNA (probe) and L/D-NIBC to covalently attach to a classic gold rod electrode by the Au−S bond (Figure 1a left). We observe the peak current at the −0.26 V (versus Ag/AgCl) of the L-surface to be about 12.0% larger than the D-surface (Figure 1b). Furthermore, the nonspecific adsorption of DNA is minimized using 6-mercapto-1-hexanol (MCH) as a spacer thiol on the gold surface.[35] We presume this difference arises due to several possibilities: (i) more DNA molecules are assembled on the L-surface than the D-surface; (ii) the distance of MB and gold electrode on the L-surface is closer than the corresponding D-surface; (iii) both (i) and (ii). In order to confirm the above hypothesis, we further investigate the covalent assembly of DNA on the L/D-surface using the QCM method (Figure 1c). The frequency shift (ΔF) of the quartz crystal resonator is nearly identical after 75 min of fabrication, hinting that the assembly amount of DNA is almost

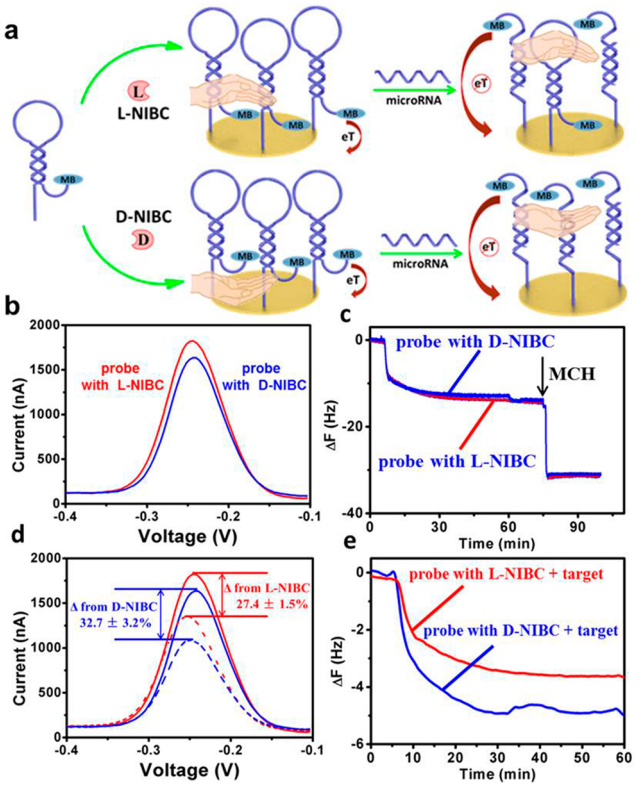

Figure 1. (a) Schematic representation of covalent assembly of DNA and hybridization on the L/D-surface. (b) Representative square-wave voltammograms (SWV) for the DNA assembly on the enantioselective gold electrodes. (c) Assembly processes of DNA on enantiomorphous gold surfaces are monitored in real-time using QCM. (d) In the absence of targets (solid lines), efficient collision between MB and the electrode produces a large faradic current. Upon addition of 100 nM microRNA (dashed lines), a signal decrease is observed. (e) Hybridization processes are monitored in real-time using QCM.

the same on the enantioselective gold surfaces; that is to say, the surface chirality has little effect on the assembly quality of the DNA. Thus, the difference of the peak current is mainly caused by the variant distance between MB and gold electrode. The interaction between DNA and chiral molecules is distinguished when DNA is anchored at gold surface by thiol. Short-chain DNA has a stronger interaction on the L-surface, which results in a closer distance between MB and the gold surface; for the D-surface, the interaction is weak, thus exhibiting a farther distance between MB and the gold surface. We presume that this result originates from a different H-bond interaction between the DNA and chiral molecule. The H-bond can be destroyed in the presence of the denaturant urea, and stem-loop structure unfolds as the concentration of urea rises. Urea titration experiments show that the D-surface unfolds priorly because of the weaker H-bond interaction (Figure S2, Supporting Information). Furthermore, the ratio of peak current (I_L/I_D) reaches its maximum when the molar ratio of NIBC to probe is 1:4 (Figure S3, Supporting Information).

According to the above conclusions, we further hybridize the DNA assembly on the L/D-surface with microRNA (Figure 1a right). Upon addition of 100 nM microRNA, a peak current decrease is observed (Figure 1d), presumably because the hybridization with a target molecule reduces the collision efficiency between MB and the interrogating electrode. More interestingly, the I_L/I_D value is increased after a 100 nM target

DOI: 10.1021/ac504797e
Anal. Chem. XXXX, XXX, XXX−XXX

addition (Figure S3, Supporting Information). The I_L/I_D value is about 1.12 in the absence of target; at the same time, the I_L/I_D value is unchanged if an equal amount of target hybridizes to the DNA on the chiral surface. However, the I_L/I_D value is increased to 1.20 in the presence of target; we deduce that fewer targets hybridize to DNA on the L-surface because of a stronger interaction between the chiral molecule with DNA. Namely, the hybridization efficiency on the L-surface is lower than the D-surface. Square-wave voltammetry (SWV) (Figure 1d) results confirm our supposition. Furthermore, we further validate this hypothesis using QCM and electron impact spectroscopy (EIS) methods. The decrease of frequency (Figure 1c) and the R_{ct} (Figure S4, Supporting Information) are almost the same in the absence of target, but the decrease of frequency of the D-surface is larger than the L-surface after a target addition (Figure 1e). Similarly, the increase of R_{ct} of the D-surface is larger than the L-surface in the presence of target, hinting that many targets hybridize to DNA on the D-surface; these results are consistent with the SWV observation. Meanwhile, the biggest difference is obtained by optimizing the experimental conditions (Figures S5−S7, Supporting Information).

To further apply the above results, we choose the E-DNA sensor as a potential platform. As shown in Figure 2a, the signal

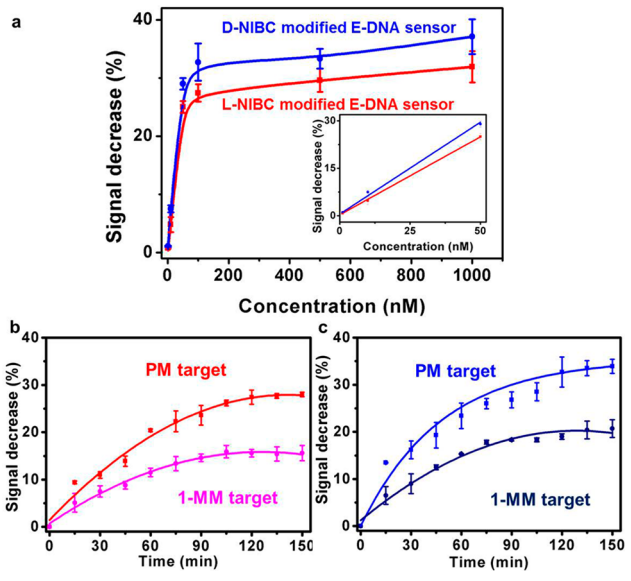

Figure 2. (a) Dose−response curves of the L-sensor (red) and D-sensor (blue). Time dependence of the L-sensor (b) and D-sensor (c) challenged with 100 nM perfectly matched (PM) target and a single-base mismatched (1-MM) target.

gain increases along with the concentration addition of perfectly matched microRNA on L(D)-NIBC modified E-DNA sensors. Significantly, we observe the hybridization efficiency of the D-NIBC modified E-DNA sensor (D-sensor) is higher than the L-sensor over the concentration range from 1 to 1000 nM after a 2 h incubation. In order to hybridize with probe, the target should first overcome the interaction force between the DNA probe and chiral molecule on the surface. The L-surface has a stronger interaction with the DNA probe; the hybridization with nucleic acids needs to overcome this strong interaction force, which results in lower hybridization efficiency. The D-surface, in contrast, has a weaker interaction with the DNA probe, resulting in higher hybridization efficiency. Furthermore, the phenomenon also exists in the presence of DNA targets (Figures S8 and S9, Supporting Information) and even when directly performed in 10% blood serum (Figure S10, Supporting Information). We deduce this result arises due to different reaction rates on enantioselective E-DNA sensors. Therefore, we further perform the reaction kinetic analysis; the rate constants are 0.053 and 0.09 min^{-1} on the L-sensor and D-sensor, respectively (Figure S11, Supporting Information), which hints that the reaction rate on the D-sensor is faster than the L-sensor in the first 10 min after the addition of DNA target (PM-51). This result is probably the reason why different hybridization efficiencies occur on enantioselective E-DNA sensors and further proves our previous conclusion. In addition, various realistic demands require a high sensitivity (a steep relationship between target concentration and output signal) such as drug monitoring with a narrow therapeutic range and logic gates.[36−39] We obtained the tunable sensitivity on enantioselective E-DNA sensors (Table S2, Supporting Information).

We also investigate the signal gain assembled with a racemic mixture of the DL-NIBC modified E-DNA sensor. The result demonstrates that the hybridization efficiency on the DL-sensor is lower than that of the D-sensor and similar to the L-sensor (Figure S12, Supporting Information). We speculate the L-NIBC first interaction with the probe on the racemic NIBC modified sensor because of the stronger interaction force between L-NIBC and the probe. Thus, the target hybridizing with the probe only needs to overcome the interaction force between L-NIBC and the probe, which results in similar efficiency with the L-NIBC modified E-DNA sensor.

In order to investigate the specific response of the enantioselective E-DNA sensors, control experiments are performed by incubating the L-/D-sensors with single-base mismatched target. As illustrated in Figure 2b,c, the enantioselective E-DNA sensors are capable of discriminating between perfectly matched target (PM target) and single-base mismatched target (1-MM target). For the L-sensor, the current is suppressed by 27.4 ± 1.5% in the presence of 100 nM PM target after a 2 h incubation; the signal is decreased by only 15.6 ± 0.8% for 1-MM target in the same conditions (Figure 2b). Similarly, for the D-sensor, the current is suppressed by 32.7 ± 3.2% and 19.0 ± 0.6% in the presence of PM target and 1-MM target, respectively (Figure 2c). Of note, we observe the signal gain of the D-sensor is higher than the L-sensor challenged with 100 nM PM target over the time range from 15 to 150 min (Figure S13a, Supporting Information). Moreover, a similar result is also observed in the presence of 1-MM target (Figure S13b, Supporting Information).

The above results confirm that molecular chirality has the ability to regulate DNA self-assembly and hybridization. However, the difference of the hybridization efficiency is not significant; this may be caused by the little DNA amount in the stem-loop probe. In order to amplify the difference, we attempt to investigate the influence of molecular chirality on the supersandwich assay, which exhibits efficient signal amplification using signal probe hybridized with two regions of a target DNA[40] (Figure 3a). We observe that there is a large difference on the limit of detection; the limit of detection on the D-NIBC modified supersandwich is 1 pM and lower than the value on the L-NIBC modified supersandwich by about 2 orders of magnitude (Figure 3b and Table 1). More excitingly, the difference of sensitivity is distinct; we observe the highest

DOI: 10.1021/ac504797e
Anal. Chem. XXXX, XXX, XXX−XXX

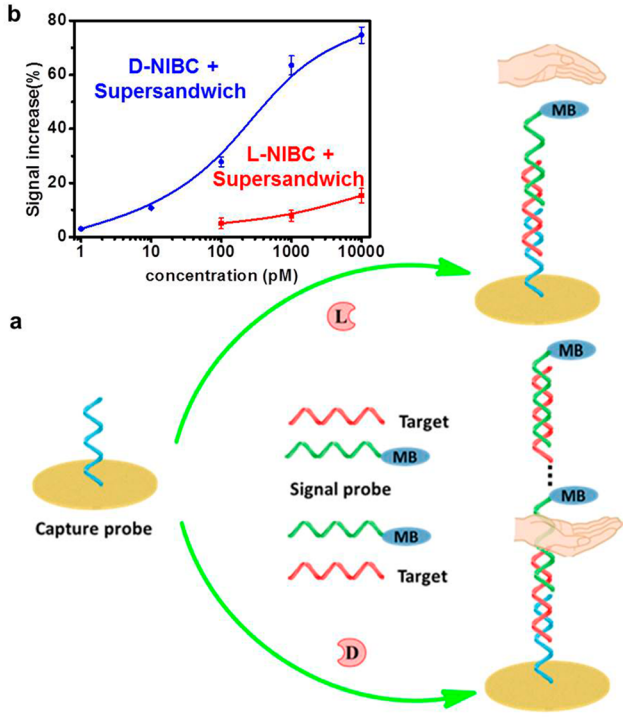

Figure 3. (a) Schematic representation of the supersandwich assay on the L-/D-NIBC modified E-DNA sensor. (b) Dose−response curves of the L-NIBC modified supersandwich (red) and D-NIBC modified supersandwich (blue).

Table 1. Dynamic Ranges of the Enantioselective Supersandwich

sensor type	sensitivity (slope of titration curve)/nM^{-1}	limit of detection/pM
L	0.92 ± 0.08	100
D	46.5 ± 6.8	1

sensitivity (46.5 nm^{-1}) when we employed D-NIBC, which is much greater than the L-NIBC coated supersandwich.

In conclusion, we regulate the DNA self-assembly and hybridization on chiral molecule modified gold surfaces. First, we prove the short-chain DNA has a larger adsorption quality on the L-surface than the D-surface. Second, we investigate the covalent assembly of DNA on enantioselective surfaces by using MB modified DNA as a model molecule; the peak current on the L-surface is larger than the D-surface. Third, we further discuss the hybridization of DNA on chiral surfaces with nucleic acid by SWV, QCM, and EIS; the results suggest that the D-surface has a larger hybridization efficiency. Fourthly, we apply the above results to an actual application by choosing the E-DNA sensor as a valuable platform. Finally, we amplify the difference of hybridization efficiency using the supersandwich assay and acquire a significant difference on the enantioselective sensors. More interestingly, our findings are successfully employed to program the sensitivity and limit of detection. Chirality is ubiquitous in living systems and very important in biochemical processes; thus, this result is significant for clinical diagnostics, gene therapy, and relevant studies.[41] On the other hand, owing to the ubiquity of the interaction between biomolecules in the living world, this result can help us to better understand the origin of chiral preference in nature.

■ ASSOCIATED CONTENT

Supporting Information

Experimental details. This material is available free of charge via the Internet at http://pubs.acs.org/.

■ AUTHOR INFORMATION

Corresponding Author

*Fax: +86-27-87559484. E-mail: xiafan@hust.edu.cn.

Notes

The authors declare no competing financial interest.

■ ACKNOWLEDGMENTS

This work was supported by National Basic Research Program of China (973 program, 2015CB932600, 2013CB933000), National Natural Science Foundation of China (21375042, 21405054) and 1000 Young Talent (to F.X.).

■ REFERENCES

(1) Sun, T.; Qing, G.; Su, B.; Jiang, L. *Chem. Soc. Rev.* **2011**, *40*, 2909−2921.
(2) Zerrouki, D.; Baudry, J.; Pine, D.; Chaikin, P.; Bibette, J. *Nature* **2008**, *455*, 380−382.
(3) Castilla, A. M.; Ramsay, W. J.; Nitschke, J. R. *Acc. Chem. Res.* **2014**, *47*, 2063−2073.
(4) Blaschke, G.; Kraft, H. P.; Fickentscher, K.; Köhler, F. *Arzneim. Forsch.* **1979**, *29*, 1640−1642.
(5) Zhao, C.; Ren, J.; Gregoliński, J.; Lisowski, J.; Qu, X. *Nucleic Acids Res.* **2012**, *40*, 8186−8196.
(6) Feng, L.; Xu, B.; Ren, J.; Zhao, C.; Qu, X. *Chem. Commun.* **2012**, *48*, 9068−9070.
(7) Wu, L.; Zhao, C.; Ren, J.; Qu, X. *Chem.—Eur. J.* **2014**, *20*, 11675−11679.
(8) Wei, W.; Qu, K.; Ren, J.; Qu, X. *Chem. Sci.* **2011**, *2*, 2050−2056.
(9) Baranes, K.; Moshe, H.; Alon, N.; Schwartz, S.; Shefi, O. *ACS Chem. Neurosci.* **2014**, *5*, 370−376.
(10) Tang, K.; Gan, H.; Li, Y.; Chi, L.; Sun, T.; Fuchs, H. *J. Am. Chem. Soc.* **2008**, *130*, 11284−11285.
(11) Gan, H.; Tang, K.; Sun, T.; Hirtz, M.; Li, Y.; Chi, L.; Butz, S.; Fuchs, H. *Angew. Chem., Int. Ed.* **2009**, *48*, 5282−5286.
(12) Sun, T.; Han, D.; Rhemann, K.; Chi, L.; Fuchs, H. *J. Am. Chem. Soc.* **2007**, *129*, 1496−1497.
(13) Hanein, D.; Geiger, B.; Addadi, L. *Science* **1994**, *263*, 1413−1416.
(14) Wang, X.; Gan, H.; Zhang, M.; Sun, T. *Langmuir* **2012**, *28*, 2791−2798.
(15) Wang, X.; Gan, H.; Sun, T. *Adv. Funct. Mater.* **2011**, *21*, 3276−3281.
(16) Qing, G.; Zhao, S.; Gong, Y.; Lv, Z.; Jiang, F.; Liu, Y.; Chen, H.; Zhang, M.; Sun, T. *J. Am. Chem. Soc.* **2014**, *136*, 10736−10742.
(17) Lee, S. J.; Lin, W. *Acc. Chem. Res.* **2008**, *41*, 521−537.
(18) Addadi, L.; Weiner, S. *Nature* **2001**, *411*, 753−755.
(19) Qing, G.; Shan, X.; Chen, W.; Lv, Z.; Xiong, P.; Sun, T. *Angew. Chem., Int. Ed.* **2014**, *53*, 2124−2129.
(20) Chen, Q.; Bae, S. C.; Granick, S. *Nature* **2011**, *469*, 381−384.
(21) Park, H.; Afzali, A.; Han, S.; Tulevski, G. S.; Franklin, A. D.; Tersoff, J.; Hannon, J. B.; Haensch, W. *Nat. Nanotechnol.* **2012**, *7*, 787−791.
(22) Bigioni, T. P.; Lin, X.; Nguyen, T. T.; Corwin, E. I.; Witten, T. A.; Jaeger, H. M. *Nat. Mater.* **2006**, *5*, 265−270.
(23) Sassolas, A.; Leca-Bouvier, B. D.; Blum, L. J. *Chem. Rev.* **2008**, *108*, 109−139.
(24) Giljohann, D. A.; Seferos, D. S.; Daniel, W. L.; Massich, M. D.; Patel, P. C.; Mirkin, C. A. *Angew. Chem., Int. Ed.* **2010**, *49*, 3280−3294.
(25) Pei, H.; Zuo, X. L.; Pan, D.; Shi, J. Y.; Huang, Q.; Fan, C. H. *NPG Asia Mater.* **2013**, *5*, e51.

DOI: 10.1021/ac504797e
Anal. Chem. XXXX, XXX, XXX−XXX

(26) Macfarlane, R. J.; Lee, B.; Jones, M. R.; Harris, N.; Schatz; Mirkin, C. A. *Science* **2011**, *334*, 204−208.
(27) Wilner, O. L.; Willner, I. *Chem. Rev.* **2012**, *112*, 2528−2556.
(28) Gennerich, A. *Nat. Nanotechnol.* **2014**, *9*, 11−12.
(29) Sharma, J.; Chhabra, R.; Cheng, A.; Brownell, J.; Liu, Y.; Yan, H. *Science* **2009**, *323*, 112−116.
(30) Wang, Z. G.; Ding, B. Q. *Acc. Chem. Res.* **2014**, *47*, 1654−1662.
(31) Fan, C. H.; Plaxco, K. W.; Heeger, A. J. *Proc. Natl. Acad. Sci. U. S. A.* **2003**, *100*, 9134−9137.
(32) Li, D.; Song, S. P.; Fan, C. H. *Acc. Chem. Res.* **2010**, *43*, 631−641.
(33) Schoukroun-Barnes, L. R.; Wagan, S.; White, R. J. *Anal. Chem.* **2014**, *86*, 1131−1137.
(34) Sauerbrey, G. *Z. Phys.* **1959**, *155*, 206−222.
(35) Herne, T. M.; Tarlov, M. J. *J. Am. Chem. Soc.* **1997**, *119*, 8916−8920.
(36) Porchetta, A.; Vallee-Belisle, A.; Plaxco, K. W.; Ricci, F. *J. Am. Chem. Soc.* **2012**, *134*, 20601−20604.
(37) Porchetta, A.; Vallee-Belisle, A.; Plaxco, K. W.; Ricci, F. *J. Am. Chem. Soc.* **2013**, *135*, 13238−13241.
(38) Xiang, Y.; Wang, Z. D.; Xing, H.; Wong, N. Y.; Lu, Y. *Anal. Chem.* **2010**, *82*, 4122−4129.
(39) Kang, D.; Vallee-Belisle, A.; Porchetta, A.; Plaxco, K. W.; Ricci, F. *Angew. Chem., Int. Ed.* **2012**, *51*, 6717−6721.
(40) Xia, F.; White, R. J.; Zuo, X. L.; Patterson, A.; Xiao, Y.; Kang, D.; Gong, X.; Plaxco, K. W.; Heeger, A. J. *J. Am. Chem. Soc.* **2010**, *132*, 14346−14348.
(41) Heller, M. J. *Annu. Rev. Biomed. Eng.* **2002**, *4*, 129−153.

DOI: 10.1021/ac504797e
Anal. Chem. XXXX, XXX, XXX−XXX